INVARIANCE OF THE VELOCITY FIELD INDUCED BY A BUBBLE RISING STEADILY THROUGH LIQUID UNDER VARIATION OF THE GAS-LIQUID DENSITY RATIO

M. Wörner

Forschungszentrum Karlsruhe GmbH
Institut für Reaktorsicherheit
Postfach 3640, 76021 Karlsruhe, GERMANY
Phone: +49 7247 82-2577, Fax: +49 7247 82-3718,
E-mail: woerner@irs.fzk.de

ABSTRACT

We investigate the influence of the density ratio on the buoyancy driven motion of a single bubble rising through still liquid by two series of volume-of-fluid simulations. In each series the values of the Morton number (Mo) and bubble Eötvös number ($Eö_B$) are fixed while the density ratio is varied, so that the liquid density is two to fifty times the gas density. The runs of series A ($Mo = 3.09 \cdot 10^{-6}$, $Eö_B = 3.06$) result in an ellipsoidal bubble, those of series B ($Mo = 266$, $Eö_B = 243$) in an ellipsoidal-cap bubble. In both cases the bubble rises along a rectilinear path. We find that the density ratio affects the bubble acceleration. Once the bubble rise is steady, the bubble shape, the bubble Reynolds number and the properly scaled bubble driven liquid motion are virtually independent of the density ratio.

1. INTRODUCTION

1.1. Motivation

Despite the enormous amount of research that has been devoted to the buoyancy-driven motion of bubbles and drops in the past, there are still some aspects that are not fully clarified. For example, the influence of the disperse-to-continuous phase density ratio (Γ_ρ) as one of the fundamental similarity parameters determining the shape and rise of fluid particles has attracted rather little attention up to now. Associated with the development of advanced methods for direct numerical simulation (DNS) of interfacial flows and the availability of more and more powerful computers there is, however, an increased interest to quantify the influence of Γ_ρ. This is because in two-phase flow a DNS is often not performed for a density ratio of about 1/1000, as it is typical for air bubbles in water. Instead, in order to avoid numerical problems and to minimize the computational costs, a density ratio of about 1/100 is often chosen. Ye et al. [1], for example note that for very small values of Γ_ρ the disparity of the fluid property across the interface makes the computation stiff and often leads to numerical instability. Bunner & Tryggvason [2] observe that their multi-grid solver fails to converge in the solution of the pressure Poisson equation if the density ratio is very small. They state that a SOR solver is more robust, but its use is impractical because it increases the computational time required to achieve the same accuracy by one to two orders of magnitude. Another drawback of values of Γ_ρ substantially different from unity is the difference in diffusive time scale of both phases. Wörner [3] reports that the maximum time step size allowed for numerical stability of an explicit time integration scheme decreases almost linear with Γ_ρ. For all these reasons it appears favorable to perform simulations with a density ratio of order 1/10 or 1/100 instead of 1/1000. This, however, raises the question to what extent results obtained from such simulations can be transferred to gas-liquid systems of higher density ratio.

1.2. Literature survey

For a fluid particle rising with its terminal velocity through an infinite liquid there are eight physical quantities of influence [4]: ρ_c^*, ρ_d^*, μ_c^*, μ_d^*, σ^*, g^*, d_B^*, V_T^*. Here ρ^* denotes the density, μ^* the dynamic viscosity, σ^* the coefficient of surface tension, g^* the acceleration of gravity, d_B^* the sphere-equivalent diameter of the fluid particle and V_T^* its terminal rise velocity. The subscripts d and c denote the dispersed and continuous phase, respectively, and * is used to indicate a dimensional quantity. These eight quantities obey three basic dimensions (length, time, mass). Dimensional analysis therefore yields that there are five independent dimensionless groups [4], namely the bubble Reynolds number (Re_B), the bubble Eötvös number ($Eö_B$), the Morton number (Mo), and the ratios of disperse-to-continuous phase density (Γ_ρ) and viscosity (Γ_μ):

$$Re_B \equiv \frac{\rho_c^* d_B^* V_T^*}{\mu_c^*}, \quad Eö_B \equiv \frac{g^*\left(\rho_c^* - \rho_d^*\right)d_B^{*2}}{\sigma^*}, \quad Mo \equiv \frac{(\rho_c^* - \rho_d^*)g^* \mu_c^{*4}}{\rho_c^{*2}\sigma^{*3}}, \quad \Gamma_\rho \equiv \frac{\rho_d^*}{\rho_c^*}, \quad \Gamma_\mu \equiv \frac{\mu_d^*}{\mu_c^*} \quad (1)$$

Therefore, there exists for example a functional relationship of type $Re_B = f(Mo, Eö_B, \Gamma_\rho, \Gamma_\mu)$. We note that any of the non-dimensional groups Re_B, Mo, $Eö_B$ can be replaced by the Weber number in virtue of the identity $We_B \equiv \rho_c^* d_B^* V_T^{*2}/\sigma^* = Re_B^2\sqrt{Mo/Eö_B}$. The set of non-dimensional groups according to Eq. (1) has the advantage that there is only one group (Re_B) that incorporates the rise velocity and only one group ($Eö_B$) that incorporates the equivalent diameter.

Experimental studies on the influence of the density ratio as a similarity parameter are rare. The reason is that Γ_ρ is not a parameter which can be easily varied in an experiment, while at the same time all the other parameters are kept constant. In the course of an experimental series, usually one specific continuous phase and various dispersed phases are used, or vice versa. In general, by this approach together with the density ratio also the viscosity ratio and the Morton number are varied. This procedure is therefore unsuited to reveal the specific functional dependence of Re_B from Γ_ρ. Nevertheless, Grace [4] notes that for bubbles rising in liquids Γ_ρ and Γ_μ tend to be very small so that the density and viscosity of the dispersed phase become unimportant causing $Re_B = f(Mo, Eö_B)$.

The specific influence of the density ratio can be investigated more easily by means of numerical simulation. Dandy & Leal [5] study the steady axisymmetric motion and deformation of a fluid particle in a streaming flow by a finite-difference scheme using the stream function-vorticity formulation of the Navier-Stokes equation and a boundary-fitted orthogonal coordinate system. The authors consider both the case of a bubble and a drop. For the bubble the viscosity ratio is 1 and the values of the Reynolds and Weber number are fixed to $Re_B = 100$, $We_B = 4$, while two values of the density ratio are considered: $\Gamma_\rho = 0.1$ and 0.01. For the drop they use $Re_B = 60$, $We_B = 4$, $\Gamma_\mu = 100$ and the values of the density ratio are $\Gamma_\rho = 10$, 100, and 1000. The authors find that the variation of the density ratio produces only a slight change in shape and flow field. They state that "the only surprise is that the effect of variation of the density ratio is so weak". Recently, Ye et al. [1] developed a combined Eulerian-Lagrangian method where the Navier-Stokes equation is solved on a fixed grid and the interface is explicitly defined by geometric curves in the computational domain. They compute the rise of an axisymmetric bubble for the same constant parameters as Dandy & Leal (i.e. $Re_B = 100$, $We_B = 4$, $\Gamma_\mu = 1$), but consider values of the density ratio that span three orders of magnitude: $\Gamma_\rho = 0.1$, 0.01, 0.001. They confirm that the differences are small, but observe that for the higher values of Γ_ρ the bubble is slightly less deformed.

Oka & Ishii [6] performed 3D level-set simulations of a single bubble rising through liquid in a square duct. They introduce the reduced Morton number $Mo^\dagger = Mo/(1 - \Gamma_\rho)$ and reduced Eötvös number $Eö^\dagger = Eö/(1 - \Gamma_\rho)$ and perform simulations for fixed values $Mo^\dagger = 3.125\cdot10^{-3}$, $Eö^\dagger = 20$ for the three different density ratios $\Gamma_\rho = 0.02$, 0.01, 0.001. They find that the effect of variation of Γ_ρ on the cap-type bubble shape and the flow field is extremely weak when Γ_ρ is smaller than 0.02. Additionally, they perform a run with $\Gamma_\rho = 0.1$ and $Mo^\dagger = 3.125\cdot10^{-3}/(1 - 0.1) = 3.472\cdot10^{-3}$ and $Eö^\dagger$

= 20 / (1 − 0.1) = 22.22. By this choice of $Mo^\dagger$ and $E\ddot{o}^\dagger$ they take into account the effect of the change of the density difference $\Delta\rho^*$ that results from variation of the density ratio and thus ensure that in all four runs the values of Mo and $E\ddot{o}_B$ are (almost) identical. Oka & Ishii [6] find that in the run with $\Gamma_\rho = 0.1$ the rise velocity is about 5.5% less than in the run with $\Gamma_\rho = 0.001$.

Bunner & Tryggvason [2] use a front-tracking method to perform simulations of 3D bubbly flow for $E\ddot{o}_B = 1$ and $Mo = 1.23\cdot10^{-6}$ using $\Gamma_\rho = 0.02$. They justify this choice by the observation that in 2D tests using much smaller density ratios the effect of the density ratio and of the inertia of the fluid inside the bubble is small for these values [7].

Sabisch et al. [8] performed 3D simulations of a single bubble rising through an initially quiescent liquid within a vertical channel by the volume-of-fluid (VOF) method. For the density ratio they used $\Gamma_\rho = 0.5$ and for the viscosity ratio $\Gamma_\mu = 1$. They considered four different combinations of ($Mo, E\ddot{o}_B$) which were chosen so that from the diagram of Clift, Grace, and Weber (CGW) [9] in which Re_B is displayed as function of ($Mo, E\ddot{o}_B$) a spherical, ellipsoidal, oblate spherical cap, and a wobbling bubble shape should be expected. Despite the density ratio 0.5, the Reynolds number, shape, rising path, and wake type of the bubble agreed qualitatively very well with the regime of CGW for all four combinations of ($Mo, E\ddot{o}_B$). From this result one may conjecture that the dependence of the bubble Reynolds number on the density ratio is weak in general, not only for $\Gamma_\rho < 0.02$. These results motivated a study by Wörner [3] who systematically investigated the influence of the density ratio on the bubble Reynolds number by a series of 3D VOF simulations with the parameters of the ellipsoidal bubble ($Mo = 3.09\cdot10^{-6}$, $E\ddot{o}_B = 3.06$, $\Gamma_\mu = 1$) but for different values of the density ratio: $\Gamma_\rho = 0.5, 0.2, 0.1, 0.02$. He found that the density ratio affects how fast the bubble accelerates from rest towards its terminal velocity. This can be explained by the added mass force [3]. However, the terminal value of the bubble Reynolds number Re_B was found to be virtually unaffected by the density ratio.

1.3. Objective

The velocity that enters into the bubble Reynolds number is the velocity of the center-of-mass of the bubble. This is an integral quantity. A question that arises is how is the influence of the density ratio on the *local* velocity field, both in the liquid and gas phase. This topic is investigated in the present paper. In section 2 we first give the non-dimensional equations governing the local motion in both phases. In these equations the five non-dimensional groups mentioned above appear. In section 3 we analyze results of direct numerical simulations obtained with the volume of fluid method for the rise of a bubble in a vertical channel. Two different cases are considered. The first corresponds to the ellipsoidal bubble of [3] and thus represents a medium Morton number system. The second case is that of a dimpled ellipsoidal cap bubble in a high Morton number system ($Mo = 266$, $E\ddot{o}_B = 243$, $\Gamma_\mu = 1$). For this case a new series of computations has been performed for three different values of the density ratio ($\Gamma_\rho = 0.5, 0.2, 0.1$). In section 4 we present the conclusions.

2. THEORY

2.1. Dimensional equations in fixed frame of reference

We consider the buoyancy driven motion of a single gas bubble rising through an immiscible fluid of infinite extend. The fluids reside in domains $\Omega_c^*(t^*) \subset \square^3, \Omega_d^*(t^*) \subset \square^3$ that change with time. Both fluids are considered to be Newtonian with constant viscosity. Also the density of each phase is assumed to be constant. Then, the motion of each fluid is described by the incompressible conservation equations for mass and momentum:

$$\nabla^* \cdot \mathbf{u}_c^* = 0, \quad \frac{\partial^* \rho_c^* \mathbf{u}_c^*}{\partial^* t^*} + \nabla^* \cdot \rho_c^* \mathbf{u}_c^* \mathbf{u}_c^* = -\nabla^* p_c^* + \mu_c^* \nabla^{*2} \mathbf{u}_c^* + \rho_c^* \mathbf{g}^*, \qquad \mathbf{x}^* \in \Omega_c^*(t^*) \qquad (2)$$

$$\nabla^* \cdot \mathbf{u}_d^* = 0, \quad \frac{\partial^* \rho_d^* \mathbf{u}_d^*}{\partial^* t^*} + \nabla^* \cdot \rho_d^* \mathbf{u}_d^* \mathbf{u}_d^* = -\nabla^* p_d^* + \mu_d^* \nabla^{*2} \mathbf{u}_d^* + \rho_d^* \mathbf{g}^*, \qquad \mathbf{x}^* \in \Omega_d^* \left(t^* \right) \tag{3}$$

Here, $\mathbf{u}_c^*$, $\mathbf{u}_d^*$ are the fluid velocities at specified time t^* and position in space $\mathbf{x}^*$ within a fixed coordinate system. For $|\mathbf{x}^*| \to \infty$ we assume the fluid of the continuous phase to be at rest.

We denote the boundary between both fluid domains by $S_i^*(t^*)$, a point on the interface by $\mathbf{x}_i^*$, and the unit normal vector pointing into the continuous phase by $\mathbf{n}_i$. We assume that the interface thickness is zero and the coefficient of surface tension is constant. At the interface we have the conditions of continuity of velocity and the continuity of normal and tangential stresses:

$$\left.\begin{aligned} \mathbf{u}_c^* = \mathbf{u}_d^* = \mathbf{u}_i^* \\ \left(p_c^* - p_d^* + \kappa^* \sigma^* \right) \mathbf{n}_i = \left[\mu_c^* (\nabla^* \mathbf{u}_c^* + \nabla^* \mathbf{u}_c^{*\mathrm{T}}) - \mu_d^* (\nabla^* \mathbf{u}_d^* + \nabla^* \mathbf{u}_d^{*\mathrm{T}}) \right] \cdot \mathbf{n}_i \end{aligned}\right\} \mathbf{x}_i^* \in S_i^*(t^*) \subset \Box^2 \tag{4}$$

Here, κ^* is twice the mean interface curvature.

The interface can be specified geometrically by the equation $F(\mathbf{x}_i^*, t^*) = 0$. As the boundary between the two fluids is a material surface, F is a quantity which is invariant for a fluid particle at the interface, so that the interface evolution is described by

$$\frac{\mathrm{D}F}{\mathrm{D}t^*} = \frac{\partial F}{\partial t^*} + \mathbf{u}_i^* \cdot \nabla^* F = 0 \tag{5}$$

We now introduce some integral quantities of the bubble and denote these by subscript "B". As the disperse phase is incompressible the volume of the fluid particle is constant in time. The bubble volume, sphere-equivalent diameter, position vector of the center-of-mass, and the translational velocity of the bubble are given by

$$\mathcal{V}_B^* \equiv \iiint_{\Omega_d^*(t^*)} \mathrm{d}V^*, \, d_B^* \equiv \left(\frac{6 \mathcal{V}_B^*}{\pi} \right)^{\frac{1}{3}}, \, \mathbf{Y}_B^*(t^*) \equiv \frac{1}{\mathcal{V}_B^*} \iiint_{\Omega_d^*(t^*)} \mathbf{x}^* \mathrm{d}V^*, \, \mathbf{V}_B^*(t^*) \equiv \frac{\mathrm{d}\mathbf{Y}_B^*(t^*)}{\mathrm{d}t^*}, V_B^*(t^*) \equiv \left| \mathbf{V}_B^*(t^*) \right| \quad (6)$$

For the analysis that will follow it is convenient to introduce a frame of reference moving with the center-of-mass of the bubble. For this purpose we make the following transformation

$$t^{*\prime} = t^*, \mathbf{z}^* = \mathbf{x}^* - \mathbf{Y}_B^*(t^*), \mathbf{w}_c^* \left(\mathbf{z}^*, t^* \right) = \mathbf{u}_c^*(\mathbf{x}^*, t^*) - \mathbf{V}_B^*(t^*), \mathbf{w}_d^* \left(\mathbf{z}^*, t^* \right) = \mathbf{u}_d^*(\mathbf{x}^*, t^*) - \mathbf{V}_B^*(t^*) \tag{7}$$

The acceleration of the moving coordinate system O' is given by $(-\,\mathrm{d}V_B^* / \mathrm{d}t^*)$. As it is well known (see e.g. [10], p. 140) the equation of motion in a moving frame is identical in form with that in an absolute frame provided that the fictitious body force per unit mass is added to the real body forces.

2.2. Non-dimensional equations in moving frame of reference

To make the above equations dimensionless we use the sphere-equivalent bubble diameter d_B^* as reference length and the bubble's center-of-mass velocity $V_B^* \neq 0$ as reference velocity. The reference time is given by d_B^*/V_B^*. As reference density and viscosity we choose the values of the continuous phase. To distinguish a non-dimensional quantity from its dimensional counterpart we use the same symbol but omit the superscript *. The non-dimensional density and viscosity of the continuous phase are then unity $\rho_c = \mu_c = 1$ while the disperse phase values are $\rho_d = \Gamma_\rho$ and $\mu_d = \Gamma_\mu$. The definition of the non-dimensional pressure is different as we incorporate in it the effect of the hydrostatic pressure of the continuous phase:

$$p_c \equiv \frac{p_c^* - \rho_c^* \mathbf{g}^* \cdot \mathbf{x}^*}{\rho_c^* V_B^{*2}}, \quad p_d \equiv \frac{p_d^* - \rho_c^* \mathbf{g}^* \cdot \mathbf{x}^*}{\rho_c^* V_B^{*2}} \tag{8}$$

Introducing the unit vector in the direction of gravity $\mathbf{n}_g \equiv \mathbf{g}^*/g^*$ the non-dimensional equations in the moving frame of reference become

$$\nabla'\cdot\mathbf{w}_c = 0, \quad \frac{\partial\mathbf{w}_c}{\partial t} + \nabla'\cdot\mathbf{w}_c\mathbf{w}_c = -\nabla'p_c + \frac{1}{Re_B}\nabla'^2\mathbf{w}_c - \frac{d\mathbf{V}_B}{dt}, \qquad \mathbf{z}\in\Omega'_c(t) \qquad (9)$$

$$\left.\begin{aligned}\nabla'\cdot\mathbf{w}_d &= 0\\[2mm]\Gamma_\rho\left(\frac{\partial\mathbf{w}_d}{\partial t} + \nabla'\cdot\mathbf{w}_d\mathbf{w}_d\right) &= -\nabla'p_d + \frac{\Gamma_\mu}{Re_B}\nabla'^2\mathbf{w}_d - \sqrt{\frac{E\ddot{o}_B^3}{MoRe_B^4}}\,\mathbf{n}_g - \Gamma_\rho\frac{d\mathbf{V}_B}{dt}\end{aligned}\right\}\;\mathbf{z}\in\Omega'_d(t) \qquad (10)$$

The conditions for $|\mathbf{z}|\to\infty$ are $\mathbf{w}_c = -\mathbf{V}_B(t)$ while those at the interface are

$$\left.\begin{aligned}\mathbf{w}_c &= \mathbf{w}_d = \mathbf{w}_i\\[2mm]\left(p_c - p_d + \kappa\sqrt{\frac{E\ddot{o}_B}{MoRe_B^4}}\right)\mathbf{n}_i &= \frac{1}{Re_B}\left[(\nabla'\mathbf{w}_c + \nabla'\mathbf{w}_c^{\mathrm{T}}) - \Gamma_\mu(\nabla'\mathbf{w}_d + \nabla'\mathbf{w}_d^{\mathrm{T}})\right]\cdot\mathbf{n}_i\end{aligned}\right\}\;\mathbf{z}_i\in S'_i(t) \qquad (11)$$

From the Eqs. (9) - (11) we see that the non-dimensional field variables p_c, p_d, $\mathbf{w}_c$, $\mathbf{w}_d$, respectively $\mathbf{u}_c$, $\mathbf{u}_d$, and the location of the interface depend on the five independent non-dimensional groups Re_B, $E\ddot{o}_B$, Mo, Γ_ρ, and Γ_μ. Unlike in section 1.2 we have received this result not by dimensional analysis but directly from the basic governing equations.

In this paper we are especially interested in the influence of the density ratio. We note that the density ratio does neither appear in the momentum equation of the continuous phase, Eq. (9), nor in the coupling condition at the interface, Eq. (11). Therefore, the influence of the density ratio is restricted to the flow within the bubble. The flow within the bubble is likely to be a circulatory one. When there is no internal flow ($\mathbf{w}_d = 0$) or in the limit $\Gamma_\rho \to 0$ the density ratio drops from Eq. (10). In this case it is thus without influence and obviously it is $Re_B = f(Mo, E\ddot{o}_B, \Gamma_\mu)$.

2.3.   Steady flow in moving frame of reference

In what follows we consider now the special case of steady motion. We assume that the bubble rises with constant velocity $V_B \neq 0$ and in the moving frame of reference the bubble shape and the flow inside and outside the bubble are steady. Then the time derivatives in Eqs. (9) and (10) cancel and the domains Ω_d' and Ω_c' are constant in time. The Navier-Stokes equation for the disperse phase then reduces to the form

$$\Gamma_\rho\nabla'\cdot\mathbf{w}_d\mathbf{w}_d = -\nabla'p_d + \frac{\Gamma_\mu}{Re_B}\nabla'\cdot\left[\nabla'\mathbf{w}_d + \nabla'\mathbf{w}_d^{\mathrm{T}}\right] - \sqrt{\frac{E\ddot{o}_B^3}{MoRe_B^4}}\,\mathbf{n}_g, \qquad \mathbf{z}\in\Omega'_d \qquad (12)$$

Making use of the generalized Gauss-Ostrogradskii divergence theorem for dyads we can integrate Eq. (12) over the domain Ω_d' and obtain

$$\iint\limits_{S'_i}\mathbf{n}_i\cdot\left\{-\Gamma_\rho\mathbf{w}_d\mathbf{w}_d - \mathbf{I}p_d + \frac{\Gamma_\mu}{Re_B}\left[\nabla'\mathbf{w}_d + \nabla'\mathbf{w}_d^{\mathrm{T}}\right]\right\}dS = \mathscr{V}_B\sqrt{\frac{E\ddot{o}_B^3}{MoRe_B^4}}\,\mathbf{n}_g \qquad (13)$$

Equation (13) is equivalent to the momentum theorem ([10], pp. 138) where the control surface is represented by the gas-liquid interface. The first term in Eq. (13) represents the convective flux of momentum out of the region bounded by S_i'. Since there is no flow across the interface it follows that this term is zero. This can readily be shown for the local term. As the terms on the left-hand-side of Eq. (13) have to be evaluated at the interface we have $\mathbf{w}_d = \mathbf{w}_i$ and thus

$$\Gamma_\rho\mathbf{n}'_i\cdot\mathbf{w}_d\mathbf{w}_d = \Gamma_\rho\mathbf{n}'_i\cdot\mathbf{w}_i\mathbf{w}_i = (\mathbf{n}'_i\cdot\mathbf{w}_i)\mathbf{w}_i = W_{i\perp}\mathbf{w}_i \qquad (14)$$

Here, $W_{i\perp}$ is the component of the interface velocity normal to the interface. As we assumed the interface position to be steady in the moving frame of reference it is $W_{i\perp} = 0$ and the momentum theorem expressed by Eq. (13) simplifies to the form

$$\iint_{S_i'} \mathbf{n}_i \cdot \left\{ -\mathbf{I} p_d + \frac{\Gamma_\mu}{Re_B} \left[\nabla' \mathbf{w}_d + \nabla' \mathbf{w}_d{}^{\mathrm{T}} \right] \right\} \mathrm{d}S = \mathcal{V}_B \sqrt{\frac{E\ddot{o}_B^3}{MoRe_B^4}} \mathbf{n}_g \tag{15}$$

Equation (15) states that there is a balance between the drag force and the buoyancy force.

The significance of the momentum theorem is that it shows that the details of the motion within the region enclosed are irrelevant and knowledge of the conditions at the surface are sufficient to describe the problem. As the gas-liquid density ratio Γ_ρ has cancelled from Eq. (15) this suggests that for steady motion and fixed bubble shape the bubble Reynolds number is a function only of Mo, $E\ddot{o}_B$, Γ_μ but not of Γ_ρ. The density ratio may, however, have an influence on the shape of the bubble. This topic is investigated in the next section by means of direct numerical simulation.

3. NUMERICAL SIMULATION RESULTS

3.1. Physical parameters

In this section we present results of direct numerical simulations. Two series of simulations for two different types of bubbles are analyzed. The physical parameters are chosen so that a steady bubble rising along a rectilinear path and an axisymmetric bubble shape should be expected. In simulation series A the value of the Morton number is $Mo = 3.09 \cdot 10^{-6}$, which is a typical value when the liquid phase is of intermediate viscosity. The value chosen for the bubble Eötvös number is $E\ddot{o}_B = 3.06$. From the CGW regime diagram [9] we expect an oblate ellipsoidal bubble. In simulations series B the value of the Morton number is $Mo = 266$ which is characteristic for a very viscous liquid. The value of the bubble Eötvös number is $E\ddot{o}_B = 243$. The parameters of series B are the same as in an experiment by Bhaga & Weber [12] where a dimpled ellipsoidal cap bubble was observed. In all our simulations the value of the viscosity ratio is fixed to unity, while the value of the density ratio is varied to investigate its influence on the simulation results.

3.2. Governing equations and numerical method

We perform the simulations in a fixed frame of reference. For tracking of the gas-liquid interface we use the volume-of-fluid method. The foundation of the method is the definition of a scalar quantity f representing the volumetric fraction of the continuous (liquid) phase within an averaging volume. Here, the averaging volume is taken to be a mesh cell. For $f = 1$ the cell is filled with liquid, for $f = 0$ it is filled with gas, while for $0 < f < 1$ both phases instantaneously coexist in the mesh cell and thus an interface is present. Based on f we define the (non-dimensional) mixture density, mixture viscosity, and center-of-mass velocity within a mesh cell:

$$\rho_m \equiv \frac{f \rho_c^* + (1-f)\rho_d^*}{\rho_c^*} = f + (1-f)\Gamma_\rho, \quad \mu_m \equiv f + (1-f)\Gamma_\mu, \quad \mathbf{u}_m \equiv \frac{1}{U_{ref}^*} \frac{f \rho_c^* \mathbf{u}_c^* + (1-f)\rho_d^* \mathbf{u}_d^*}{f \rho_c^* + (1-f)\rho_d^*} \tag{16}$$

Based on above quantities the equations governing the motion in the continuous phase (Eq. (2)), in the disperse phase (Eq. (3)), and the coupling condition (Eq. (4)) can be combined into one single continuity and momentum equation valid in the entire domain $\Omega = \Omega_c \cup \Omega_d$ (see [11]):

$$\nabla \cdot \mathbf{u}_m = 0 \tag{17}$$

$$\frac{\partial \rho_m \mathbf{u}_m}{\partial t} + \nabla \cdot \rho_m \mathbf{u}_m \mathbf{u}_m = -\nabla p + \frac{1}{Re_{ref}} \nabla \cdot \mu_m \left[\nabla \mathbf{u}_m + \nabla \mathbf{u}_m{}^{\mathrm{T}} \right] - (1-f)\frac{E\ddot{o}_{ref}}{We_{ref}} \mathbf{n}_g + \frac{\kappa a_i \mathbf{n}_i}{We_{ref}} \tag{18}$$

Here a_i is the non-dimensional interfacial area within the averaging volume. The above equations are made dimensionless by a reference length L_{ref}^* and a reference velocity U_{ref}^*. Based on these scales - equivalent to the definitions of Re_B, $E\ddot{o}_B$, We_B in section 1.2 - a reference Reynolds number (Re_{ref}), reference Eötvös number ($E\ddot{o}_{ref}$), and reference Weber number (We_{ref}) can be defined. The set of equations is completed by the transport equation for the liquid volumetric fraction

$$\frac{\partial f}{\partial t} + \nabla \cdot \left(f \mathbf{u}_m \right) = 0 \tag{19}$$

For the solution of Eq. (19) by the VOF method we have developed the interface reconstruction algorithm EPIRA which belongs to the class of PLIC (Piecewise Linear Interface Calculation) methods. Equations (17) and (18) are discretized employing a regular staggered grid and second order central differences. The solution strategy is based on a projection method and a third order Runge-Kutta time integration method. Details about the numerical method can be found in [8].

3.3. Computational set up

Figure 1 shows the coordinate system and a sketch of the computational domain. The x-, y- and z-axes are assigned in vertical, transverse, and wall-normal direction, respectively. The gravity vector points in negative x-direction. In x- and y-direction we have periodic boundary conditions; at $z = 0$ and $z = 1$ we have rigid walls and no-slip boundary conditions. The size of the computational domain in terms of L_{ref}^* is $2 \times 1 \times 1$. This domain is discretized by $128 \times 64 \times 64$ uniform mesh cells. A spherical bubble with diameter 0.25 is positioned in the domain with its center located at (0.5, 0.5, 0.5). The overall void fraction is about 0.4 %. Both, liquid and gas are initially at rest.

To perform the simulations we must specify the reference quantities. We use $L_{ref}^* = 4$ m, $U_{ref}^* = 1$ ms^{-1}, $g^* = 9.81$ ms^{-2}. To determine the values of the reference Eötvös, Weber, and Reynolds number in the Navier-Stokes Eq. (18) we proceed as follows. Choosing a certain value for the density ratio and taking the values for Mo and $E\ddot{o}_B$ given above we successively compute

$$E\ddot{o}_{ref} = \left(\frac{L_{ref}^*}{d_B^*} \right)^2 E\ddot{o}_B, \quad We_{ref} = \frac{E\ddot{o}_{ref}}{1 - \Gamma_\rho} \frac{U_{ref}^{*\,2}}{g^* L_{ref}^*}, \quad Re_{ref} = \left(\frac{E\ddot{o}_{ref} We_{ref}^2}{Mo} \right)^{0.25} \tag{20}$$

In Table I we give these input values for the different density ratios considered in the present study. Additionally, we give the values of We_{ref} and Re_{ref} for the asymptotic case $\Gamma_\rho \to 0$.
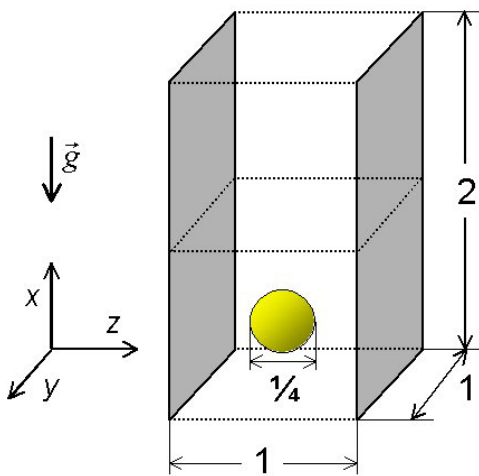

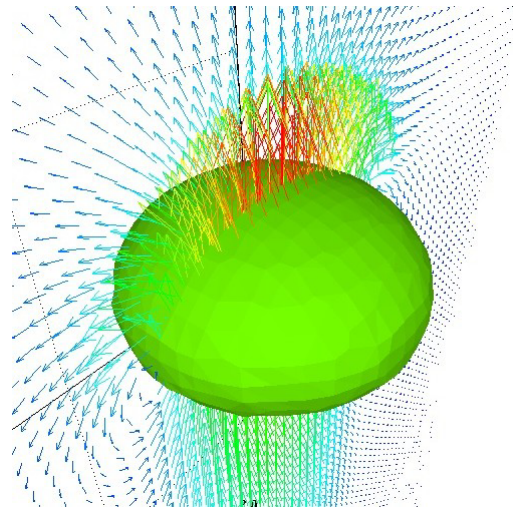Figure 1: Sketch of coordinate system and computational domain.

Figure 2: Instantaneous bubble shape and velocity vectors in plane $y = 0.5$ for run A50.

Run	Γ_ρ	$1/\Gamma_\rho$	$E\ddot{o}_{ref}$	We_{ref}	Re_{ref}	Δt	N_T
A2	0.5	2	49.05	2.5	100.00	0.0005	1,100
A5	0.2	5	49.05	1.5625	78.90	0.0003	1,800
A10	0.1	10	49.05	1.3888	74.39	0.00015	3,200
A50	0.02	50	49.05	1.2755	71.29	0.00003	13,000
	0	∞	49.05	1.25	70.57		
B2	0.5	2	3,888	792.7	55.05	0.0005	5,000
B5	0.2	5	3,888	495.4	43.52	0.0001	17,000
B10	0.1	10	3,888	440.4	41.03	0.0001	16,000
	0	∞	3,888	396.3	38.93		

3.4. Bubble Reynolds number

In Fig. 3 the time history of the vertical position of the bubble center-of-mass is shown for all simulations of series A and B. It is apparent that the density ratio affects how fast the bubble accelerates from rest towards its terminal velocity and also affects the specific value of the terminal velocity. This behavior can be explained by the added mass force [3]. Figure 4, however, shows that the terminal value of the bubble Reynolds number Re_B is obviously unaffected by the density ratio. In case A the value of the terminal bubble Reynolds number is about 56. As shown in [3] this value is in good agreement with that of a correlation $Re_B = f(Mo, E\ddot{o})$ obtained from two-phase wave theory [13]. In case B Re_B is about 6.5 and thus is about 16% smaller than in the experiment [12], where $Re_B = 7.77$. We attribute the lower value in the simulation to the influence of the viscosity ratio which is here unity but in the experiment is estimated to be about 10^{-5}.
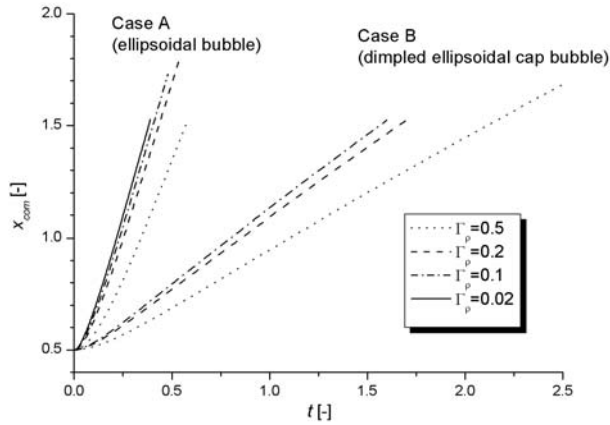

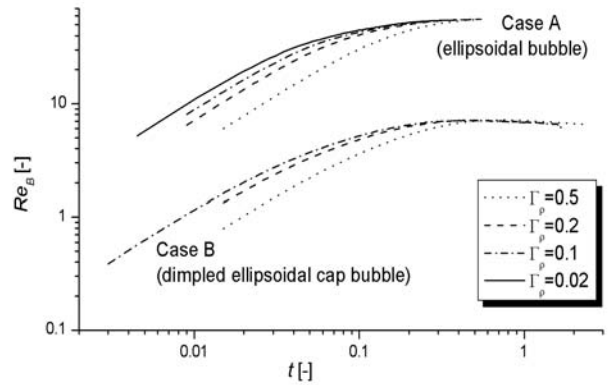Figure 3: Time history of vertical position of bubble center-of-mass (x_{com}).

Figure 4: Time history of bubble Reynolds number.

3.5. Bubble shape

Figure 2 shows a snapshot of the bubble shape for run A50. As expected the bubble is of oblate ellipsoidal shape. The steady bubble shape for run B2 is displayed in Figure 5. For a better visualization of the dimpled ellipsoidal shape only the back half of the bubble is shown. Figure 6 shows the experimental bubble shape reproduced from [12]. Though in the simulation the density ratio is $\Gamma_\rho = 0.5$ and in the experiment it is $\Gamma_\rho = 0.0008$ the bubble shapes in Figs. 5 and 6 are quite similar. However, one can identify a small difference in curvature at the bottom of the bubble.

We now make a quantitative comparison of the bubble shape for the runs of case A and B. We consider that instant in time when the vertical position of the bubble center-of-mass is x_{com} = 1.5 and thus the bubble has moved four times its initial diameter. Note that this time level differs from run to run (see Fig. 3). In Table II we give the ratios of the bubble dimensions a_x, a_y, a_z for the different runs. We see that the influence of the density ratio on the bubble dimensions is surprisingly small. However, as Γ_ρ decreases the values of a_x/a_y and a_x/a_z slightly increase in case A and thus the bubble is less oblate. This is in agreement with the numerical findings of Ye et al. [1]. For case B the trend is opposite. The ratio of the horizontal dimensions a_x/a_y is always close to unity indicating that the bubble is axisymmetric. Note that in our 3D simulations on a Cartesian grid no assumption regarding axisymmetry is involved. In most cases the ratio a_y/a_z is larger than 1 so that the bubble dimension in span-wise direction is slightly larger than in wall-normal direction. This indicates that the walls are not sufficiently far away to have any influence. Nevertheless, we conclude that neither in case A nor in case B the density ratio has any major influence on the bubble shape.

Table II: Ratios of the bubble dimensions.

Γ_ρ	$1 / \Gamma_\rho$	Case A			Case B		
		a_x / a_y	a_x / a_z	a_y / a_z	a_x / a_y	a_x / a_z	a_y / a_z
0.5	2	0.648	0.659	1.017	0.538	0.556	1.033
0.2	5	0.652	0.665	1.021	0.528	0.544	1.030
0.1	10	0.658	0.669	1.016	0.528	0.543	1.029
0.02	50	0.668	0.666	0.998	-	-	-

Figure 5: Computed bubble shape for run B2 (only the back half of the bubble is shown).

Figure 6: Experimental bubble shape reproduced from [12].

3.6. Local velocity profiles

We now compare local velocity profiles along a certain line within the flow domain. In Fig. 7 the vertical velocity component u is shown as function of the vertical co-ordinate x for fixed span-wise and wall-normal co-ordinates $y = z = 0.492$ for the runs of series A. Additionally, in Fig. 7 the profile of the liquid volumetric fraction is displayed to indicate the bubble position ($f = 0$). While the profiles of f almost collapse to a single curve, the profiles of u are similar, but do not collapse. The latter result is not really surprising since in all runs the velocity is normalized by the same value $U_{ref}^* = 1$ ms^{-1}. From the analysis in section 2 we expect similarity of the velocity field when it is scaled by the bubble rise velocity. In Fig. 8 we show the velocity profiles normalized by the bubble rise velocity of the respective run and indeed find that the profiles collapse to a single curve.

In Fig. 9 the profiles of f and the scaled vertical velocity u/V_B are shown along the wall-normal coordinate. This figure illustrates the internal circulation within the bubble. Inside the bubble at z = 0.5 we can identify a small effect of the density ratio on the velocity profile. However, within the liquid phase the profiles again collapse to a single curve. This also holds for the wall-normal profile of the scaled wall-normal velocity u/V_B at a position within the bubble wake, see Fig. 10.
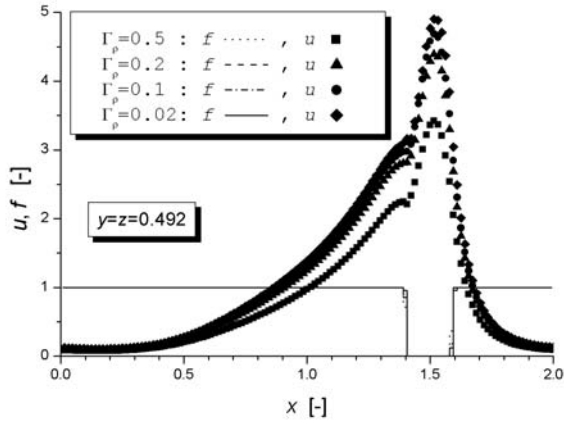
Figure 7: Vertical profile of local instantaneous vertical velocity, u, and liquid volume fraction, f, for case A and $y = z = 0.492$.
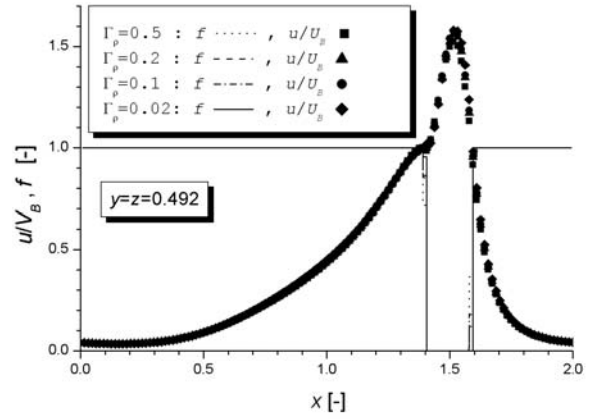

Figure 8: Vertical profile of normalized local instantaneous vertical velocity u/V_B and liquid volume fraction, f, for case A and $y = z = 0.492$.
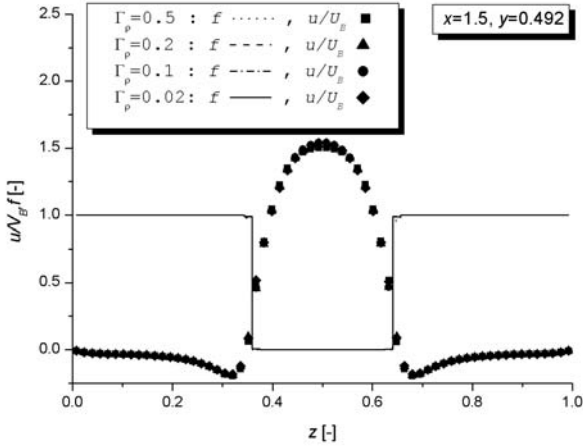

Figure 9: Wall-normal profile of scaled vertical velocity, u/V_B, and liquid volume fraction, f, for case A and $x = 1.5$, $y = 0.492$.
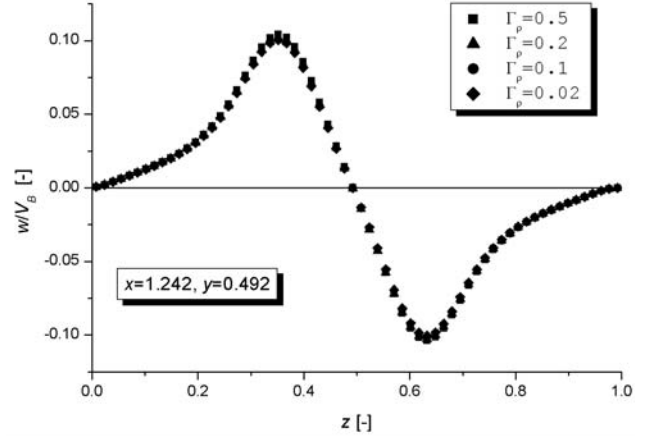

Figure 10: Wall-normal profile of scaled wall-normal velocity w/V_B for case A and $x = 1.242$, $y = 0.492$ (bubble wake).
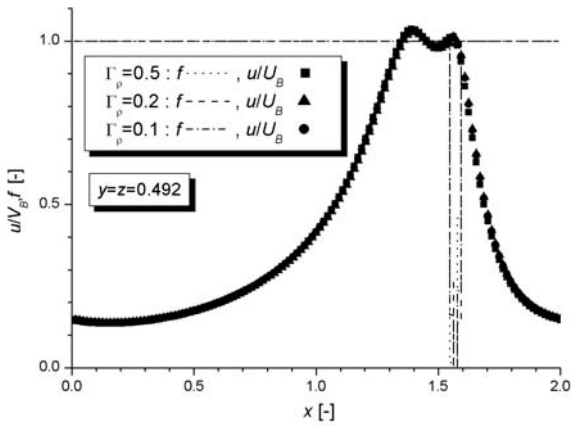

Figure 11: Vertical profile of normalized local vertical velocity u/V_B and liquid volume fraction, f, for case B and $y = z = 0.492$.
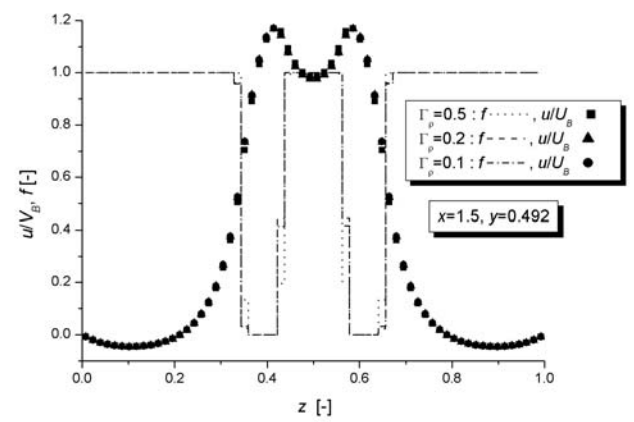

Figure 12: Wall-normal profile of scaled vertical velocity, u/V_B, and liquid volume fraction, f, for case B and $x = 1.5$, $y = 0.492$.

In Figs. 11 and 12, we show similar graphs as in Figs. 8 and 9 but for case B. Again we find that the scaled velocity profiles are independent of Γ_ρ. However, the profiles for case A and B clearly differ. For case A, the value of u/V_B at $x = 0$ and $x = 2$ in Fig. 8 is about 0.05. For case B this value is about 0.15, see Fig. 11. This value can be considered to give a measure on the influence of the periodic boundary conditions applied in vertical direction. The rather high value in case B indicates that the bubble already may experience the influence of the "leading" bubble. In case B the bubble's center-of-mass lies - due to the dimpled ellipsoidal shape - within the liquid phase. As a consequence the wall-normal profile of the vertical velocity exhibits a local minimum, see Fig. 12.

4. CONCLUSIONS

In the present paper the influence of the gas-liquid density ratio (Γ_ρ) on the buoyancy driven motion of a single bubble is investigated theoretically and numerically. Using the volume-of-fluid method for tracking the gas-liquid interface, two series of simulation series are performed for fixed values of the Morton number and the bubble Eötvös number and a unity viscosity ratio. Case A ($Mo = 3.09 \cdot 10^{-6}$, $Eö_B = 3.06$) corresponds to a liquid phase of intermediate viscosity while case B ($Mo = 266$, $Eö_B = 243$) corresponds to a very viscous liquid. In each simulation series various density ratios are considered, namely 0.5, 0.2, 0.1 and (only in case A) 0.02. After an initial transient, all simulations result in steady bubbles rising along a rectilinear path. In case A the bubble shape is oblate ellipsoidal, in case B it is of ellipsoidal-cap type. The results show that the density ratio has a notable influence on the initial acceleration of the bubble. Once the bubble reached its terminal velocity, however, the bubble shape and Reynolds number are virtually independent of the density ratio. This also holds for the local velocity field induced by the rising bubble within the liquid phase, when scaled by the bubble rise velocity. For case A a minor influence of the density ratio on the internal motion within the bubble is identified. We find the computed bubble shape of case B to be in good agreement with an experiment [12] performed for the same values of Mo and $Eö_B$ but for a density ratio of 1/1300 and a viscosity ratio of about 10^{-5}.

At present the invariance of the density ratio for steady rising single bubbles is demonstrated only for the specific parameters of $Eö_B$, Mo, and Γ_μ given above. However, the simulations cover two orders of magnitude in the bubble Eötvös number, eight orders of magnitude in the Morton number and one order of magnitude in the bubble Reynolds number which is about 56 in case A and 6.5 in case B. We therefore expect that for steady bubbles the influence of the density ratio is marginal in general. For such bubbles then rather universal relations for bubble Reynolds number and drag coefficient in terms of Mo and $Eö_B$ should exist. Furthermore, the scaling of the bubble driven liquid motion suggests that rather universal models may be derived in terms of Mo and $Eö_B$ also for the pseudo-turbulence induced by bubbles rising almost steadily in dilute gas-liquid flows. Finally, we conclude that for steady bubbles it is possible to perform computationally efficient direct simulations with density ratio of order 0.1 while the results can be transferred to gas-liquid systems with density ratio of order 0.001.

It would be interesting to verify the invariance of the density ratio experimentally. This requires measurements with at least two sets of different gas-liquid or liquid-liquid systems which have the same Morton number but a different density ratio. If the Morton number of both systems is the same, then similarity of the Eötvös number can be ensured by properly setting the bubble diameters.

NOMENCLATURE

a_i	interfacial area concentration	Γ_μ	gas-liquid viscosity ratio
a_x, a_y, a_z	bubble dimensions	Γ_ρ	gas-liquid density ratio
d_B	bubble diameter	κ	interface curvature
$Eö$	Eötvös number	μ	dynamic viscosity

f	liquid volumetric fraction	ρ	density
g	gravity	σ	coefficient of surface tension
L_{ref}	reference length	Superscripts	
Mo	Morton number	$*$	dimensional variable
$\mathbf{n}$	unit normal vector	$'$	coordinate system in moving frame
p	pressure		of reference
Re	Reynolds number	Subscripts	
t	time	B	bubble
$\mathbf{V}_B, V_B$	bubble velocity	c	continuous phase (liquid)
U_{ref}	reference velocity	com	center-of-mass
$\mathbf{u}, \mathbf{w}$	velocity vectors	d	disperse phase (gas)
u, v, w	velocity components	i	interface
We	Weber number	m	mixture value
$\mathbf{x}, \mathbf{z}$	position vectors	ref	reference value

REFERENCES

[1] Ye, T., Shyy, W., & Chung, J.N., A fixed-grid, sharp-interface method for bubble dynamics and phase change, J. Comput. Phys., 174, pp. 781-815, 2001.

[2] Bunner, B., & Tryggvason, G., Dynamics of homogeneous bubbly flows. Part I: Motion of the bubbles. Submitted to Journal of Fluid Mechanics.

[3] Wörner, M., The influence of gas-liquid density ratio on shape and rise velocity of an ellipsoidal bubble: A numerical study by 3D volume-of-fluid computations, F.-P. Schindler (Hrsg.), VDI Forschritt-Berichte, Reihe 3, Nr. 738, pp. 67-84, VDI Verlag Düsseldorf, ISBN 3-18-373803-1, 2002.

[4] Grace, J.R., Shapes and velocities of bubbles rising in infinite liquids, Trans. Instn. Chem. Eng., 51, pp. 116-120, 1973.

[5] Dandy, D.S., & Leal, L.G., Buoyancy-driven motion of a deformable drop through a quiescent liquid at intermediate Reynolds number, J. Fluid Mech., 208, pp. 161-192, 1989.

[6] Oka, H., & Ishii, K., Numerical analysis on the motion of gas bubbles using level set method, J. Physical Soc. Japan, 68, pp. 823-832, 1999.

[7] Tryggvason, G., Bunner, B., Ebrat, O., & Tauber, W., Computations of multiphase flows by a finite difference/front tracking method. I. Multifluid flows, Von Karman lecture notes , the von Karman Institute, 1998.

[8] Sabisch, W., Wörner, M., Grötzbach, G., & Cacuci, D.G., 3D volume-of-fluid simulation of a wobbling bubble in a gas-liquid system of low Morton number, 4th Int. Conf. on Multiphase Flow, New Orleans, LA, U.S.A., CD-ROM, paper 244, May 27 - June 1, 2001.

[9] Clift, R., Grace, J.R., & Weber, M.E., Bubbles, Drops, and Particles, Academic Press, 1978.

[10] Batchelor, G.K., An introduction to fluid dynamics, Cambridge Univ. Press, Reprint 1970.

[11] Wörner, M., Sabisch, W., Grötzbach, G., & Cacuci, D.G., Volume-averaged conservation equations for volume-of-fluid interface tracking, 4th Int. Conf. on Multiphase Flow (ICMF), New Orleans, LA, U.S.A., CD-ROM, paper 245, May 27 - June 1, 2001.

[12] Bhaga, D., & Weber, M.E., Bubbles in viscous liquids: shapes, wakes and velocities, J. Fluid Mech., 105, pp. 61-85, 1981.

[13] Mendelson, H.D., The prediction of Bubble Terminal Velocities from Wave Theory, AIChE Journal, 13, pp. 250-253, 1967.